Hybrid Graphene/Gold Plasmonic Fiber-Optic Biosensor

*Nancy Meng Ying Zhang, Kaiwei Li, Perry Ping Shum, Xuechao Yu, Shuwen Zeng, Zhifang Wu, Qi Jie Wang, Ken Tye Yong, and Lei Wei**

The emergence of 2D materials starts a new chapter of optical, electrochemical, and nanoelectronic sensors, owing to their unique optical, electrical, mechanical, structural, and chemical properties and atomically thin thickness.[1] In particular, 2D materials exhibit superior optical properties such as universal optical conductivity, broadband absorption from visible to infrared frequency, and novel gate-tunable plasmonic properties.[2] Therefore, integrating 2D materials into conventional optical sensors delivers unprecedented enhancement on sensing performance. There are mainly two ways that 2D materials are integrated into optical sensors. The most straightforward one is to simply place 2D material on the surface of a waveguide or a prism to utilize the optical absorption or plasmonic property by replacing the commonly used metallic thin films to gain a better sensing characteristic.[3–6] The other way is to integrate the 2D material into a plasmonic sensor to tune or enhance the resonant property, as well as serve as a functional layer. For example, integrating 2D materials into a conventional surface plasmon (SP) resonance sensor could construct plasmonic metasurfaces.[7] Moreover, recent studies have explored the great potential of 2D material/metal hybrid film-like structures for the sensitivity enhancement on conventional Kretschmann configuration based plasmonic sensor.[7–19] Various hybrid plasmonic sensing platforms have been proposed, such as graphene/gold,[7–10] graphene oxide/gold,[11–15] graphene-MoS_2/gold,[16–18] and MX_2/silicon/gold.[19] However, most of these studies are preliminary theoretical investigations.

In this work, we study the influence of 2D material on hybrid plasmonic photonic structure on the surface plasmon polariton (SPP) excitation as well as the sensing performance of this hybrid plasmonic sensor. To be more specific, we take optical fiber, the most prevalent form of dielectric waveguide as a model to carry out eigenmode analysis to investigate the drift of resonant coupling between TM-polarized guided mode and SPP induced by the additional atomic layer on metal film. As it is unrealistic to discuss all existing 2D materials in details, our analysis concentrates on graphene, which is the most representative and commercially available 2D material. In addition to their superior optical properties, graphene has also been demonstrated to be an excellent functionalization strategy. The honeycomb arrangement of carbon atoms forms π-stacking interaction with aromatic rings that commonly exist in biomolecules.[20] Besides, as the plasmonic sensitivity is critically decayed as the thickness of functionalization layer increases,[21] the atomically thin graphene hardly compromises the sensing performance. More importantly, the additional graphene layer strengthens the electric field of SPP, thereby further promotes the interaction between biomolecules and evanescent field. Here, we numerically analyze and experimentally demonstrate an optical fiber based plasmonic biosensor seamlessly integrated with the graphene-on-gold hybrid structure. To validate the resulting sensor, we detect the concentration of single-stranded DNA (ssDNA), as ssDNA quantitation is a critical process in many biomedical techniques, such as DNA sequencing, cloning, gene expression, and polymerase chain reaction (PCR).[22] Our proposed biosensor provides a detection limit of 24-mer ssDNA as low as 1×10^{-12} M and a linear response within a wide range of concentrations from 1×10^{-12} to 10×10^{-6} M.

Figure 1 illustrates the configuration of our proposed biosensor. Considering the cylindrical geometry of optical fiber is not suitable for the transfer of large-area single-layer graphene, we propose to use a side-polished fiber of which the flat polished facet can better preserve the integrity as well as prevent the wrinkles of graphene sheet. To do so, a standard single-mode fiber (SMF) is laterally polished to expose the evanescent field of core mode and a thin gold film is coated on the side-polished facet. Single sheet of graphene is then transferred on top of the gold film to enhance the excited SPP as well as to bond with biomolecules. A polychromatic light source couples into the fiber core. The peak transmission loss of the output spectrum occurs at the resonance at which the phase matching condition is satisfied.[23] We use both wavelength and intensity interrogations to characterize the plasmonic behaviors. Graphene is particularly helpful for the immobilization of ssDNA molecules. Driven by the strong π-stacking interaction between aromatic carbons of graphene and nucleobases, the flexible ssDNA molecules intend to maximize the affinity, thus "lie" on the graphene surface.[20] Therefore, the entire molecules could fully interact with the surface plasmon and lead to the increase of local refractive index. As a result, the phase matching point will experience a redshift.

We first carry out numerical analysis to verify that the graphene enhanced plasmonic sensor provides better performance even for bulk refractive index sensing (see the simulation method in the Experimental Section). In the first scenario,

N. M. Y. Zhang, Dr. K. Li, Prof. P. P. Shum, Dr. X. Yu, Dr. S. Zeng, Dr. Z. Wu, Prof. Q. J. Wang, Prof. K. T. Yong, Prof. L. Wei
School of Electrical and Electronic Engineering
Nanyang Technological University
50 Nanyang Avenue, Singapore 639798, Singapore
E-mail: wei.lei@ntu.edu.sg

N. M. Y. Zhang, Dr. K. Li, Prof. P. P. Shum, Dr. X. Yu, Dr. S. Zeng, Dr. Z. Wu, Prof. Q. Jie Wang, Prof. K. T. Yong, Prof. L. Wei
CINTRA CNRS/NTU/THALES
UMI3288
Research Techno Plaza
50 Nanyang Drive, Singapore 637553, Singapore

DOI: 10.1002/admt.201600185

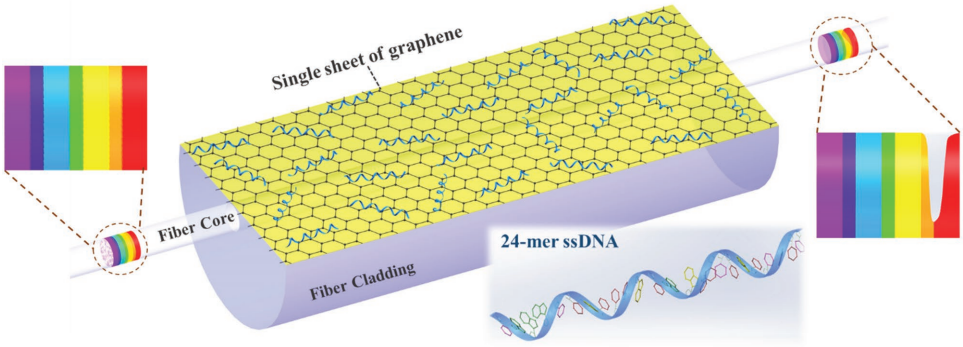

Figure 1. Proposed graphene-on-gold hybrid plasmonic biosensor. ssDNA molecules are adsorbed on single sheet of graphene through π-stacking interactions between the aromatic rings of nucleobases and honeycomb latticed carbon atoms.

a 30 nm gold film (see the discussion of gold thickness in Section S2, Supporting Information), beyond which is dielectric liquid medium, is coated on top of the side-polished facet. The black curve in **Figure 2**a shows the normalized electric field distribution of SPP excited by thin gold film. The zero position is the boundary between gold film and side-polished facet. The inset of Figure 2a plots the electric field distributions over the entire simulated configuration, which includes the dielectric medium, thin gold film, fiber core, and fiber cladding. In agreement with theory, the electric field of guided core mode is Gaussian distributed and that of SPP is the strongest at the thin film surface and exponentially decays into the dielectric medium. We add single layer of graphene on top of the gold film in the following scenario. As shown by the red curve in Figure 2a, the intensity of SPP considerably enhances by ≈30.2% with the addition of single graphene sheet. We also investigate the impact of multiple graphene layers on the plasmonic behaviors. Two or more graphene layers would depress the SPP intensity instead of further boosting it. The increase of graphene layers leads to the gradual decrease of SPP due to the energy loss of electrons induced by additional graphene layers.[7] Therefore, single sheet of graphene provides an optimal sensitivity to the change of dielectric medium (see Section S3, Supporting Information, for details).

The transmission spectra of the core modes of two scenarios are plotted in Figure 2b. The inset of Figure 2b shows the mode profiles of fundamental core mode and SP mode. With a graphene layer added, the peak transmission loss enhances, meanwhile shifts to a longer wavelength. The peak loss enhancement is due to the increased SPP excitation caused by graphene as explained above. The redshift of resonant wavelength is owing to the high refractive index of graphene, which is $3 + i\frac{C}{3}\lambda$ within visible range, where C = 5.446 μm^{-1}.[24] As the refractive index of analyte increases, the graphene enhanced sensor undergoes a larger wavelength redshift as well as a larger peak loss enhancement, leading to the improved sensitivities in both wavelength and intensity interrogations. Figure 2c,d compares the sensitivities corresponding to both wavelength and intensity interrogations when the analyte refractive index increases from 1.333 (the refractive index of numerous aqueous solutions) to 1.3505 (the refractive index of blood plasma).[25] The proposed graphene-on-gold hybrid structure improves the wavelength interrogation sensitivity from 904.49 to 1039.18 nm RIU^{-1}, and the intensity interrogation sensitivity improves from −752.62 to −897.15% RIU^{-1}. The response of plasmonic biosensor to analyte refractive index is therefore effectively promoted, which is profited from the alteration of electronic properties when graphene is deposited on metal substrate. Pristine graphene is a zero-bandgap semiconductor with valence and conduction bands touching at the conical points.[26] When graphene, of which work function is 4.5 eV, is in contact with a metal with work function higher than 5.4 eV (e.g., gold with work function of 5.54 eV), it becomes p-type doped as electrons transfer from graphene to metal surface to equilibrate the Fermi levels.[27,28] The charge transfer enhances the resonant electron oscillations at gold surface, thereby boosts the field of SPP.[7]

To fabricate the side-polished fiber, we fix a standard SMF in the groove of a silica block using epoxy. We then polish the entire silica block till the fiber core is exposed. The inset of Figure 2e illustrates the cross section of our fabricated side-polished fiber. The polished facet is further coated with a 30 nm gold film by electron beam evaporation (see the discussion of gold thickness in Section S2, Supporting Information). We characterize the plasmonic behaviors of the resulting gold-coated side-polished fiber (the experimental setup is described in the Experimental Section). The gold-coated side-polished facet sequentially immerses in refractive index matching liquids, which are NaCl solutions with different concentrations with the refractive indices ranging from 1.3326 to 1.3497. Figure 2e shows the characterization results. The resonant wavelength shifts to longer wavelengths and the peak loss enhances along with increasing analyte refractive index. As plotted in Figure 2f, both resonant wavelength shift and transmission minimum show linear relations against analyte refractive index. This phenomenon matches with the above-mentioned simulation results. The corresponding sensitivities of wavelength and intensity interrogations are 413.79 nm RIU^{-1} and −391.02% RIU^{-1}, respectively. The experimental sensitivities are less than those of simulation due to the structural differences between the fabricated fiber sensor and constructed simulation model. In the simulation, the constructed 2D model assumes perfect uniformity along the longitudinal direction of fiber and the surfaces of side-polished facet and thin gold film are perfectly planar. In the experiment, however, the polishing depth is not uniform along the longitudinal direction of fiber

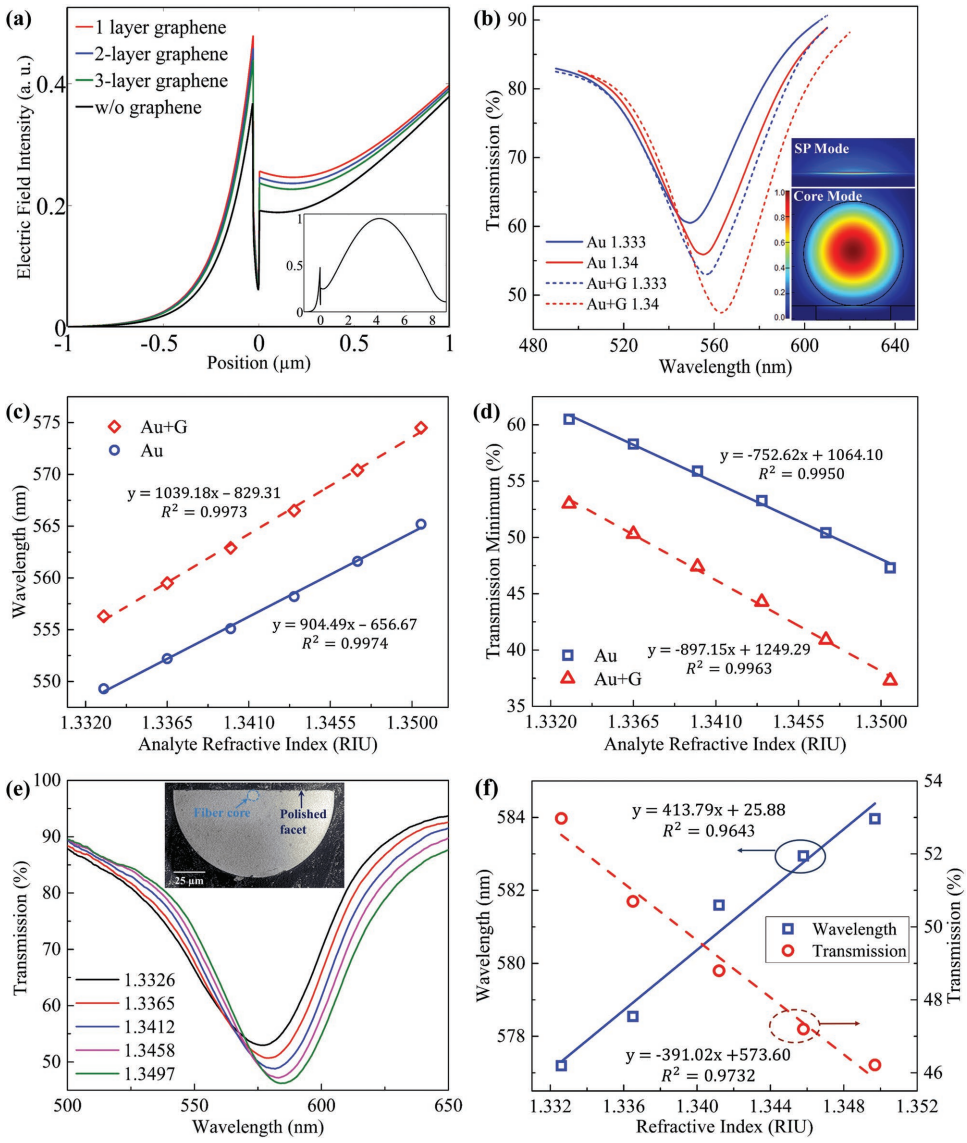

Figure 2. a) Normalized electric field intensities of excited SPPs when no graphene layer, single-layer graphene, two-layer graphene, and three-layer graphene are deposited on the 30 nm gold film coated on the side-polished facet of fiber. (Inset) Distributions of normalized electric field intensity over the entire simulated geometry. b) Transmission spectra of side-polished optical fiber based plasmonic sensors with and without single-layer graphene. (Inset) Mode profiles of the fundamental core mode and surface plasmon mode. Comparison of sensitivities between plasmonic sensors with and without single-layer graphene using c) wavelength interrogation and d) intensity interrogation. e) Transmission spectra of a side-polished fiber based plasmonic sensor with gold thickness of 30 nm. (Inset) SEM image of the cross section of the side-polished fiber. f) Measured sensitivities that correspond to wavelength and intensity interrogations.

(see Section S5, Supporting Information, for the schematic diagram of side-polished fiber) and surface roughness is measured to be around 5 nm using atomic force microscopy (AFM) (see Section S4, Supporting Information, for the AFM image). As a consequence, the sensitivities are degraded due to the uneven polishing depth[29] and surface roughness.[30–32]

Following the characterization, we transfer single sheet of graphene on top of the thin gold film by the wet transfer approach (see the Experimental Section).[33] **Figure 3**a,b shows the Raman spectra of the monolayer chemical vapor deposition (CVD)-grown graphene on copper foil and the monolayer graphene transferred onto the gold-coated side-polished optical fiber, respectively. The peak locations of G and 2D bands are at 1589 $cm^{-1} \pm 2$ cm^{-1} and 2678 $cm^{-1} \pm 2$ cm^{-1}, respectively, (see more details in Section S6, Supporting Information). The intensity ratios of 2D to G peaks in Figure 3a,b are 2.70 and 2.26, respectively, which indicate the monolayer of graphene.[34] The inset of Figure 3c shows the microscopic view of the transferred single graphene sheet boundary on the side-polished facet. The strip in the middle is the groove of silica block in which the SMF is fixed with epoxy. Figure 3c compares the transmission spectra of plain gold film and graphene-coated gold film on side-polished fiber when immerging in deionized (DI) water. In agreement with simulation, the resonant wavelength

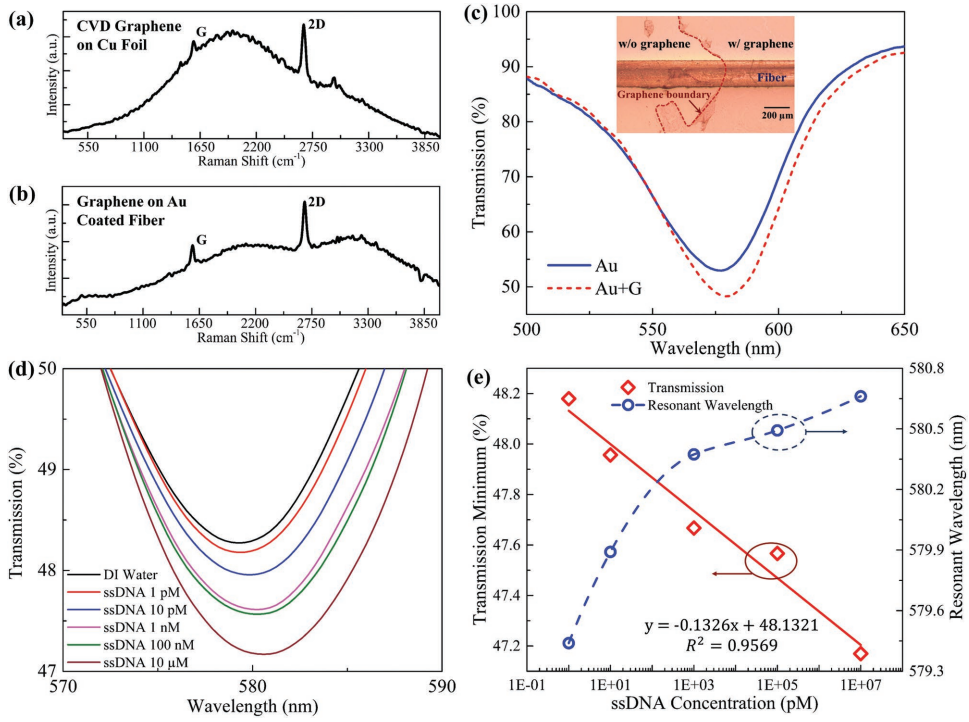

Figure 3. a) Raman spectrum of monolayer CVD-grown graphene on copper foil. b) Raman spectrum of transferred monolayer graphene on gold-coated fiber. c) Comparison of transmission spectra of configurations with and without graphene. (Inset) Microscopic view of the graphene sheet transferred on fiber. Red dotted line indicates the boundary of graphene sheet. d) Change of transmission spectra of graphene enhanced plasmonic fiber sensor when detecting concentrations of ssDNA. e) Transmission minimum and resonant wavelength against ssDNA concentrations (log $\times 10^{-12}$ M).

undergoes a redshift from 577.2 to 579.3 nm with the addition of a graphene layer. Meanwhile, the graphene sheet obviously decreases the transmission minimum from 52.97% to 48.27%. One reason why the transmission spectrum change after graphene transfer in experiment is less than that in simulation is because the sensitivity of the fabricated fiber sensor is smaller than the simulated sensitivities as we explained above. Another reason is due to the impurities associated with graphene transfer. Compared with the seamless contact between graphene and gold film, the unavoidable residual Cu atoms trapped within the graphene layer after etching leads to the imperfect contact between graphene and gold layer.[35] Also, surface roughness associated with side-polished fiber fabrication and gold film deposition degrades the contact between two materials. Hence, the transmission spectrum is less varied after graphene transfer. The decrease of transmission minimum after graphene transfer indicates a stronger excitation of SPP thereby a higher sensitivity (see the comparison and detailed discussion of plasmonic sensors with and without graphene in Section S4, Supporting Information).

Finally, we validate the biosensing capability of our proposed sensor by detecting 7.3 kDa 24-mer (5′-CTT CTG TCT TGA TGT TTG TCA AAC-3′) ssDNA (Integrated DNA Technologies) with concentrations ranging from 1×10^{-12} to 10×10^{-6} M using the same setup with aforementioned characterization. 24-mer is a commonly used oligonucleotide probe length in the detection of human disease-causing peptides and bacteria such as amyloid-β peptide,[36] *Streptococcus pyogenes*,[37] Enterobacteriaceae,[38] and *Arcobacter butzleri*.[39] We inject ssDNA solutions into flow chamber that envelops the sensing area of side-polished fiber (see schematic diagram of the flow chamber in Section S5, Supporting Information). For each concentration, we fill up the chamber with ssDNA solution and wait for 8 min to ensure that ssDNA molecules fully interact with graphene. Then we inject DI water into the flow chamber to flush away the unbonded or weakly adsorbed ssDNA molecules. We recorded the stabilized transmission spectrum at this point since only strongly adsorbed ssDNA molecules remained in the solution. Figure 3d plots the magnified transmission spectra with various ssDNA concentrations. Same with the trend when sensing bulk refractive index, the resonant dip deepens and also shifts to longer wavelengths as the concentration increases. This phenomenon is caused by the adsorption of ssDNA molecules on graphene sheet. The bonding of ssDNA varies the local refractive index as well as scatters the evanescent field, thereby causes higher transmission loss. Also, the propagation constant of SPP is modified so that the phase matching condition is satisfied at a longer wavelength.[8] We also observe a distinguishable enhancement of peak transmission loss when ssDNA concentrations is as small as 1×10^{-12} M. Such low limit of detection is benefited from the enhanced plasmonic sensitivity as well as the stable bonding between ssDNA molecules and graphene at the SPP propagation surface. Compared with a bare gold film which has weaker adsorption capability, graphene/gold hybrid structure boosts the detection limit for orders of magnitude (see Section S5, Supporting Information, for detailed analysis). Figure 3e plots the linearly decreasing transmission minimum and the gradually saturated increasing

resonant wavelength against log $\times 10^{-12}$ M concentration. Therefore, transmission minimum is adopted as the sensing parameter, and our proposed biosensor provides a linear response over a wide detection range of log scale ssDNA concentration from 1×10^{-12} to 10×10^{-6} M.

In summary, we demonstrate a graphene/gold sensing film coated optical fiber as a proof-of-concept of hybrid plasmonic waveguide biosensor. We prove by both numerical analysis and experimental demonstration that the deposition of graphene on the thin gold film coated fiber effectively enhances the excited SPP, thus promotes the sensitivities in both wavelength and intensity interrogations. Coupled with biomolecules adsorption capability, 2D material based hybrid plasmonic waveguide sensor delivers distinctive sensing performance, leading to the realization of the prospect of highly sensitive, highly integrated, flexible, and miniaturized in situ biosensors. This new sensing platform could be more versatile and the sensing performance can be further improved by introducing various nanomaterials in the future.

Experimental Section

Optical Simulation: Numerical analysis was carried out using the mode analysis in Lumerical FDTD Solutions. In the simulation, the fiber core diameter is 8 µm and the polished fiber cladding facet just coincides with the perimeter of fiber core. The refractive indices of fiber core and cladding were set based on the Sellmeier equations of fused silica and 3.5% GeO_2-doped silica, respectively.[40] The optical constants of gold and graphene are built-in parameters in Lumerical.

Experiment Setup: The same setup was used for the characterization of gold-coated side-polished fiber and the ssDNA detection. A polychromatic light source with the wavelength range from 400 to 700 nm transmits through a linear polarizer and couples into the SMF. The output light is received by a spectrometer with spectral resolution of 0.38 nm. The angle of linear polarizer is adjusted meanwhile monitoring the transmission spectrum of side-polished fiber. When the peak transmission loss on spectrum reaches the lowest point, the angle of polarizer is fixed as it corresponds to the TM-polarized core mode. Then the analyte liquids sequentially flow through the sensing area of side-polished fiber. A 532 nm Raman system (WITec alpha300) was used to measure the Raman spectra of monolayer graphene before and after wet transfer. The laser has an output power of 5 mW. The spot size is ≈500 nm focused by 100× objective lens.

Graphene Transfer Procedure: A commercial 1 cm × 1 cm single-layer graphene grown on copper foil via CVD was used. First, a few hundred nanometers of polymethyl methacrylate (PMMA) thin film was spin-coated on the top surface of graphene sheet. After the PMMA film is solidified, the whole copper foil was floated on 8.33% ammonium persulfate $(NH_4)_2S_2O_8$ solution to etch the copper foil beneath graphene. Then the remaining PMMA-coated graphene sheet was transferred to float on DI water for several times to remove the residual ions. The floating graphene sheet was located on top of gold-coated side-polished facet of the fiber, and gradually lifted out of water with the graphene sheet attached on the side-polished facet. After drying the graphene-coated fiber in 37 °C oven for 12 h, the PMMA thin film was removed by acetone.

Supporting Information

Supporting Information is available from the Wiley Online Library or from the author.

Acknowledgements

This work was supported in part by the Singapore Ministry of Education Academic Research Fund Tier 2 (MOE2015-T2-1-066, MOE2015-T2-2-010, and MOE2014-T2-1-076) and Nanyang Technological University (Start-up grant: L.W.).

Received: August 19, 2016
Revised: September 23, 2016
Published online: December 19, 2016

[1] X. Li, J. Zhu, B. Wei, *Chem. Soc. Rev.* **2016**, *45*, 3145.
[2] E. J. Lee, S. Y. Choi, H. Jeong, N. H. Park, W. Yim, M. H. Kim, J.-K. Park, S. Son, S. Bae, S. J. Kim, K. Lee, Y. H. Ahn, K. J. Ahn, B. H. Hong, J.-Y. Park, F. Rotermund, D.-I. Yeom, *Nat. Commun.* **2015**, *6*, 6851.
[3] M. F. Ubeid, M. M. Shabat, *Appl. Phys. A: Mater. Sci. Process.* **2014**, *118*, 1113.
[4] A. A. Shabaneh, S. H. Girei, P. T. Arasu, W. B. W. A. Rahman, A. A. A. Bakar, A. Z. Sadek, H. N. Lim, N. M. Huang, M. H. Yaacob, *Opt. Commun.* **2014**, *331*, 320.
[5] S. C. Yan, B. C. Zheng, J. H. Chen, F. Xu, Y. Q. Lu, *Appl. Phys. Lett.* **2015**, *107*, 053502.
[6] F. Xing, G. X. Meng, Q. Zhang, L. T. Pan, P. Wang, Z. B. Liu, W. S. Jiang, Y. Chen, J. G. Tian, *Nano Lett.* **2014**, *14*, 3563.
[7] S. Zeng, K. V. Sreekanth, J. Shang, T. Yu, C. K. Chen, F. Yin, D. Baillargeat, P. Coquet, H. P. Ho, A. V. Kabashin, K. T. Yong, *Adv. Mater.* **2015**, *27*, 6163.
[8] L. Wu, H. S. Chu, W. S. Koh, E. P. Li, *Opt. Express* **2010**, *18*, 14395.
[9] S. H. El-Gohary, N.-H. Kim, K. M. Byun, *J. Nanophotonics* **2013**, *7*, 073799.
[10] O. Salihoglu, S. Balci, C. Kocabas, *Appl. Phys. Lett.* **2012**, *100*, 213110.
[11] T. Y. Xue, S. S. Yu, X. M. Zhang, X. Z. Zhang, L. Wang, Q. L. Bao, C. Y. Chen, W. T. Zheng, X. Q. Cui, *Sci. Rep.* **2016**, *6*, 21254.
[12] N. F. Chiu, S. Y. Fan, C. D. Yang, T. Y. Huang, *Biosens. Bioelectron.* **2017**, *89*, 370.
[13] B. Meshginqalam, H. Toloue, M. T. Ahmadi, A. Sabatyan, A. Centeno, R. Ismail, *Opt. Quantum Electron.* **2016**, *48*, 328.
[14] H. Zhang, Y. Sun, S. Gao, J. Zhang, H. Zhang, D. Song, *Small* **2013**, *9*, 2537.
[15] Y. Ryu, S. Moon, Y. Oh, Y. Kim, T. Lee, D. H. Kim, D. Kim, *Appl. Opt.* **2014**, *53*, 1419.
[16] J. B. Maurya, Y. K. Prajapati, V. Singh, J. P. Saini, R. Tripathi, *Opt. Quantum Electron.* **2015**, *47*, 3599.
[17] S. Zeng, S. Hu, J. Xia, T. Anderson, X.-Q. Dinh, X.-M. Meng, P. Coquet, K.-T. Yong, *Sens. Actuators, B* **2015**, *207*, 801.
[18] J. B. Maurya, Y. K. Prajapati, V. Singh, J. P. Saini, *Appl. Phys. A* **2015**, *121*, 525.
[19] Q. Ouyang, S. Zeng, L. Jiang, L. Hong, G. Xu, X.-Q. Dinh, J. Qian, S. He, J. Qu, P. Coquet, K.-T. Yong, *Sci. Rep.* **2016**, *6*, 28190.
[20] B. Song, D. Li, W. Qi, M. Elstner, C. Fan, H. Fang, *ChemPhysChem* **2010**, *11*, 585.
[21] S. Tadepalli, Z. Kuang, Q. Jiang, K.-K. Liu, M. A. Fisher, J. J. Morrissey, E. D. Kharasch, J. M. Slocik, R. R. Naik, S. Singamaneni, *Sci. Rep.* **2015**, *5*, 16206.
[22] S. Bhat, N. Curach, T. Mostyn, G. S. Bains, K. R. Griffiths, K. R. Emslie, *Anal. Chem.* **2010**, *82*, 7185.
[23] X. Yu, Y. Zhang, S. Pan, P. Shum, M. Yan, Y. Leviatan, C. Li, *J. Opt.* **2009**, *12*, 015005.

[24] M. Bruna, S. Borini, *Appl. Phys. Lett.* **2009**, *94*, 031901.
[25] A. G. Borovoi, E. I. Naats, U. G. Oppel, *J. Biomed. Opt.* **1998**, *3*, 364.
[26] H. Liu, Y. Liu, D. Zhu, *J. Mater. Chem.* **2011**, *21*, 3335.
[27] P. A. Khomyakov, G. Giovannetti, P. C. Rusu, G. Brocks, J. Van Den Brink, P. J. Kelly, *Phys. Rev. B: Condens. Matter Mater. Phys.* **2009**, *79*, 1.
[28] G. Giovannetti, P. A. Khomyakov, G. Brocks, V. M. Karpan, J. Van Den Brink, P. J. Kelly, *Phys. Rev. Lett.* **2008**, *101*, 026803.
[29] Z. Tan, X. Hao, Y. Shao, Y. Chen, X. Li, P. Fan, *Opt. Express* **2014**, *22*, 15049.
[30] D. L. Mills, *Phys. Rev. B* **1975**, *12*, 4036.
[31] K. M. Byun, S. J. Yoon, D. Kim, *Appl. Opt.* **2008**, *47*, 5886.
[32] M. Pan, *M.Phil. Thesis*, University of Birmingham, UK **2010**.
[33] X. Li, Y. Zhu, W. Cai, M. Borysiak, B. Han, D. Chen, R. D. Piner, L. Colomba, R. S. Ruoff, *Nano Lett.* **2009**, *9*, 4359.
[34] X. Li, W. Cai, J. An, S. Kim, J. Nah, D. Yang, R. Piner, A. Velamakanni, I. Jung, E. Tutuc, S. K. Banerjee, L. Colombo, R. S. Ruoff, *Science* **2009**, *324*, 1312.
[35] G. Lupina, J. Kitzmann, I. Costina, M. Lukosius, C. Wenger, A. Wolff, S. Vaziri, M. Östling, I. Pasternak, A. Krajewska, W. Strupinski, S. Kataria, A. Gahoi, M. C. Lemme, G. Ruhl, G. Zoth, O. Luxenhofer, W. Mehr, *ACS Nano* **2015**, *9*, 4776.
[36] A. Kumar, K. M. Pate, M. A. Moss, D. N. Dean, V. Rangachari, *PLoS One* **2014**, *9*, e111492.
[37] L. N. Cella, W. Chen, N. V. Myung, A. Mulchandani, *J. Am. Chem. Soc.* **2010**, *132*, 5024.
[38] M. Ootsubo, T. Shimizu, R. Tanaka, T. Sawabe, K. Tajima, M. Yoshimizu, Y. Ezura, T. Ezaki, H. Oyaizu, *J. Appl. Microbiol.* **2002**, *93*, 60.
[39] I. V. Wesley, L. Schroeder-Tucker, A. L. Baetz, F. E. Dewhirst, B. J. Paster, *J. Clin. Microbiol.* **1995**, *33*, 1691.
[40] C.-H. Chen, R. O. Reynolds, A. Kost, *Appl. Opt.* **2006**, *45*, 519.